Instabilities and multiple steady states of radio-frequency discharges in CF_4

Efimia Metsi,[1,2] Evangelos Gogolides,[1,*] and Andreas Boudouvis[2]
[1]*Institute of Microelectronics, National Center for Scientific Research NCSR ''Demokritos,'' P.O. Box 60228, Aghia Paraskevi Attiki 15310, Greece*
[2]*Department of Chemical Engineering, National Technical University of Athens, Zografou Campus, Attiki 15773, Greece*
(Received 15 September 1995)

A one-dimensional fluid model coupled with solution tracking algorithms was applied for an $L=5$ mm CF_4 (radio frequency) rf discharge at $P=2$ Torr (low PL value of $PL=1$). The discharge exhibited a rich behavior of solution multiplicity as a function of applied rf current density (or voltage). The most prominent characteristic was the development of dc self-bias and asymmetry under completely symmetric discharge conditions, in agreement with experimental data by J. Butterbaugh (Ph.D. dissertation, Massachusetts Institute of Technology, 1990). The plasma can exist in three states of positive, negative, and zero self-bias, of which the first two are asymmetric and stable, while the third is symmetric and unstable. The two asymmetric solutions collapse again into one symmetric solution with zero self-bias at a higher voltage, a transition which depends on the value of the secondary electron emission coefficient. At lower applied currents (or voltages) the hysterisis loop of this electronegative plasma is presented between breakdown and extinction, and an unstable plasma is found between the two points. The observed phenomena are related to the transition of the discharge from diffusion-controlled to electron-oscillation-amplitude-controlled breakdowns. The sustaining mechanisms of the plasma and the electron dynamics are discussed. [S1063-651X(96)10806-0]

PACS number(s): 52.80.Pi, 52.65.Kj

I. INTRODUCTION

Multiple solutions, both stable and unstable, at a particular value of a plasma parameter (e.g., current through the discharge) are a consequence of the nonlinear nature of the plasma. A lot of work has been done with instabilities in dc discharges of electropositive (nonattaching or weakly attaching) gases. For example, as the current through a dc discharge increases, the transition from subnormal to normal and then to abnormal regimes occurs. The transition is accompanied by discharge constriction [2], and spot formation [2,3]; in addition, at certain values of the circuit parameters oscillations can occur [2,4–6].

Electronegative gases, on the other hand, are much more interesting for processing of materials. Daniels, Franklin, and Snell [7] and Franklin, Daniels, and Snell [8] presented a detailed study of the positive column in discharges of electronegative gases, and studied the radial profiles of electrons and ions for various degrees of attachment, detachment, and recombination. They showed that electronegative gas discharges form an inner ion-ion plasma, surrounded by an outer electron-ion plasma. Coulter and Emeleus [9] described the subnormal to abnormal transition of the electronegative discharges, revealing phenomena analogous to electropositive plasmas, such as constriction [10], and the moving or standing striations also studied by Woolsey *et al.* [11]. Nigham and Wiegand [12] presented a detailed analysis of the electron ionization-attachment-detachment-induced changes in the discharge, and the development of striations as a consequence of such volume processes. All of the above mentioned studies were conducted in dc discharges, and the observed phenomena are two dimensional in nature, although ionization-attachment-detachment-induced effects can be one dimensional.

The similarities between dc and rf discharges in the γ regime have been presented by Raizer and Shneider [13], but such analogies are not as obvious in the α regime. However, for rf electronegative gases the time-averaging procedure of Kaganovich [14] has many analogies with the dc work of Refs. [7] and [8]: Two main plasma regions are identified, i.e., ion-ion and electron-ion regions; depending on the value of the product (attachment frequency times ion drift time through an electrode boundary layer), the boundary layer can contain only electron-ion or electron-ion and ion-ion plasmas. Limited work has been done on the multiplicity and stability analysis of rf discharges, yet rf plasmas show even richer phenomena such as constriction and formation of plasmoids [15], period doubling [16], and ionization-attachment-detachment-induced instabilities [17]. Some of these effects are two dimensional and others one dimensional in nature. Both, however, are important as they cause nonuniformity, damage, and irreproducibility during processing of materials. Simulation of the observed effects can been done using fluid models coupled with solution tracking algorithms [18,19]. Fluid models have proved successful for the study of multiple solutions and solution branches, such as the ignition-extinction characteristics of an Ar plasma [18–20], and the onset of ionization-attachment-detachment instabilities due to electron detachment from CF_x radicals in CF_4 plasmas [17].

In a geometrically symmetric capacitively coupled rf discharge, the applied potential is divided symmetrically between the electrodes, the discharge is symmetric with respect to the two electrodes, and the dc bias is zero [21]. However, Butterbaugh [1] has recently shown that, in a narrow-gap symmetric plasma in CF_4, the symmetric discharge loses

*Author to whom all correspondence should be address. Electronic address: evgog@cyclades.nrcps.ariadne-t.gr

stability, yielding an asymmetric discharge with a dc self-bias. Analogous dc bias formation was noticed for SF_6/N_2 [22,23] at lower frequency and larger electrode gap.

Thus the purpose of this work is to examine narrow-gap discharges in CF_4, and to study and clarify the discharge sustaining mechanisms, the stability, and the solution multiplicity. This is accomplished using a one-dimensional fluid model [17–20]. In Sec. II we briefly discuss the mathematical methods employed. In Sec. III we present and discuss our results for a CF_4 plasma as a function of the magnitude of the applied sinusoidal rf current density. For convenience we divide our study into three areas: low, medium, and high current density. For low currents the hysterisis loop of breakdown extinction of the plasma is shown; for medium currents the development of dc bias under symmetric conditions is discussed; finally for high currents the disappearance of the dc bias is demonstrated. All along, a comparison with experimental data [1] is performed.

II. MATHEMATICAL METHODS AND INPUT PARAMETERS

The one-dimensional fluid model uses mass, momentum, and energy balances for electrons, mass, and momentum balances for the ions and the Poisson equation for the electric field, and is described in detail in Refs. [18] and [20]. The differential equations are discretized in space with second-order-accurate finite differences using a uniform mesh, and the resulting differential-algebraic equations are integrated using a second-order-accurate time-implicit algorithm. A shooting algorithm is used to find directly the oscillatory steady state to the applied sinusoidal rf current density [20], and is coupled with solution tracking algorithms to find solutions as a function of external parameters [19,20]. The model has already been applied for CF_4 discharges in combination with physics and chemistry models to study the plasma physics [17] and chemistry [24] (see also Refs. [17] and [24] for detailed presentation of the parameters used for CF_4).

In this work solution tracking is done with arclength continuation [25], either with an augmented Jacobian or with Keller's bordering algorithm [26]. At bifurcation points the tangent vector is used to move the solution from the old branch to a new one resulting from the bifurcation [27]. The stability of the solutions is determined from the Floquet multipliers [28,29], i.e., the eigenvalues of the Jacobian matrix of the shooting algorithm. The stability is also confirmed by applying a small perturbation in the solution, and integrating in time; stable solutions are attracted back into the branch, and unstable ones move to a more stable branch.

The input parameters used for the model are listed in Table I of Gogolides, Stathakopoulos, and Boudouvis [17]. Electron detachment from negative ions occurs via collisions with CF_x radicals, their fractional density determining the extent of electronegativity predicted for CF_4 [17,24]. A ratio CF_x to CF_4 of 10^{-3} was used in this work. Higher fractional values will result in lower negative ion densities [17], showing the large effect of plasma chemistry on plasma physics for this gas [24]. Electron mobility (times pressure) μP in CF_4 has a constant value of 20 m^2 Torr/V s at reduced electric fields (E/P) higher than 6000 V/m Torr, and *increases sharply* at lower fields (140 m^2 Torr/V s at 800 V/m Torr). The functionality of μP (and all reaction constants as well) vs E/P is converted to a functionality with respect to the average electron energy ε, and as such it is input in the fluid model, in order to avoid assumptions of local equilibrium with the electric field [18]. This implies that electron mobility in CF_4 will be high when electrons have low energy, e.g., by cooling when diffusing against the electric field. For the electron diffusivity, an Einstein relation was considered ($D/\mu = 2\varepsilon/3$), as well as a constant diffusivity. Since the electron diffusion flux (due to both density and temperature gradients) is multiplied by the ratio $D/\varepsilon = 2\mu/3$, [18] the diffusive flux is expected to be greatly enhanced in regions of the sheath where electrons are cool. The above remarks should be kept in mind when trying to explain some of the observed phenomena in the following sections. Secondary emission is included by adding a flux ($-\gamma j_+$) to the electron flux, where j_+ is the ion flux on the electrode, and γ is the secondary electron emission coefficient. The energy of emitted electrons is arbitrarily taken to be 1 eV at the electrode.

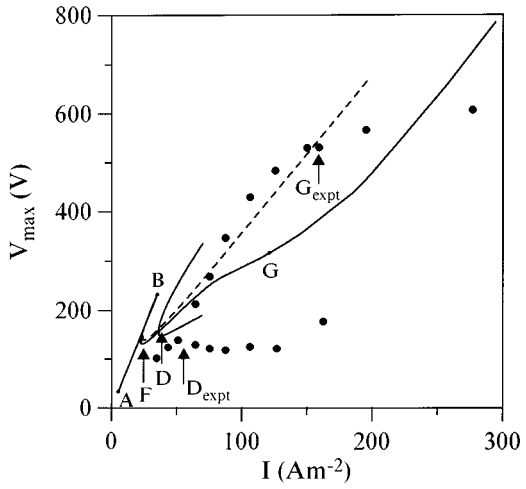

FIG. 1. Voltage-current density (V-I) characteristics of a CF_4 discharge at 5-mm spacing, 2 Torr, and 13.56 MHz. The maximum voltage ($V_{max}=V_{rf}+V_{dc}$) is shown as a function of current density amplitude. Lines denote model results (full line for $\gamma=0.1$, dashed line for $\gamma=0.01$), and symbols experimental data [1]. F and B are turning points, while A, D, and G are bifurcation points. D_{expt} and G_{expt} refer to the analogous experimental points. The symmetric solution DG is unstable between D and G, and becomes stable after G, while experimental data have the same behavior after G_{expt}.

III. RESULTS

A. Overview

An overview of the current-voltage characteristics of a 5-mm CF_4 discharge at 2 Torr is presented in Fig. 1, which shows the maximum voltage as a function of current density amplitude. For a system with no dc bias the maximum voltage is simply the amplitude of the rf voltage V_{rf}; for a system with dc bias the maximum voltage is $V_{rf}+V_{dc}$. In the same figure, the experimental results of Butterbaugh [1] are shown for a first comparison. It is thus clear that the narrow gap (or low $PL=1$) discharge exhibits a pitchfork

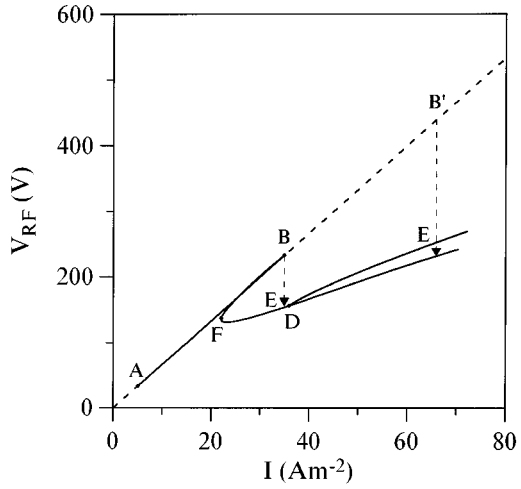

FIG. 2. *V-I* characteristics of the CF_4 discharge, at low-medium currents. Contrary to Fig. 1, the RF voltage amplitude (V_{rf}) vs the amplitude of the current density is shown. Thus the two branches with positive-negative dc bias (on the right-hand side of point *D*) fall on top of each other and above the symmetric solution *V-I* curve. *B* and *B′* are the breakdown points for $\gamma=0.1$ and 0.01, respectively. *DFBE* or *DFB′E* define a hysterisis loop.

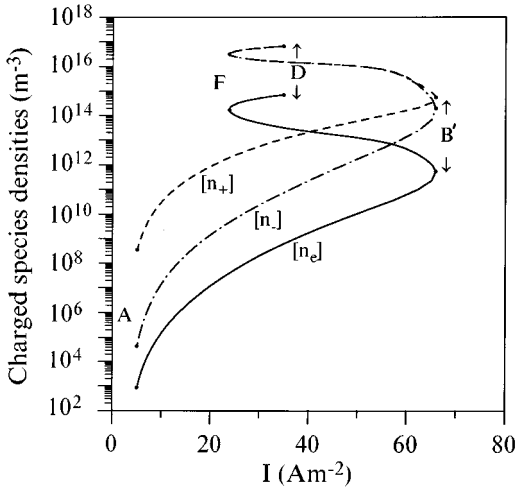

FIG. 3. Electron and ion densities vs current density for the branches *DF*, *FB′*, and *B′A*. *F* is the extinction of the plasma, and *B′* the breakdown. Densities become zero at point *A*.

bifurcation at point *D* on the *V-I* curve, resulting in branches with positive or negative dc self-bias in a symmetric system. The phenomenon takes place at medium currents, and is studied in Sec. III C. At high currents the secondary electron emission coefficient plays a significant role, as discussed in Sec. III D. At low currents two turning points F and B define the hysterisis loop of the extinction breakdown of the discharge, as described in Sec. III B.

B. Low current density regime

We now focus on the low current density region of Fig. 1, shown also in Fig. 2, and examine the discharged behavior in regions *DF*, *FB*, or *FB′*, and *BA* or *B′A*, where *B* and *B′* are the breakdown points for $\gamma=0.1$ and 0.01, respectively. Figure 2 shows the rf voltage amplitude versus rf current density amplitude in the lower current regime; in contrast with Fig. 1, only V_{rf} is plotted, and thus the two branches with dc bias starting from *D* fall on top of each other. Figure 3 shows the charged species densities in the center of the plasma as a function of current density. The part of the curve *DF* is the usual symmetric discharge, without dc bias [17,18]. In this region electron densities are lower than ion densities, while positive and negative ion densities are of almost equal magnitude. This is illustrated in Fig. 4(a), which shows the time-averaged densities of the charged species versus interelectrode position, also revealing the presence of an inner positive-negative ion plasma, and an outer electron-positive ion plasma [7,8]. The presence and form of those two plasma regions is also confirmed by the value of the product (attachment frequency times ion drift time through the electrode boundary layer) which equals $0.04 \ll 1$ [14]. Observe in Figs. 2 and 3 that as the current density forced through the discharge decreases, the densities decrease and, at point *F*, where the *V-I* and $n_e/n_+/n_-$-*I* curves turn, the plasma extinguishes. At this point the electron sheath collapses (i.e., becomes greater than half the discharge length), and electron densities drop much faster than ion densities. Sheath widths are defined as the distance from the electrode, where carrier density (electrons or ions) has increased up to a fixed, small percentage of the bulk carrier density. Because electrons oscillate, we refer to their maximum sheath width, which corresponds to the maximum oscillation of the electron front. In contrast, the ion sheath width is constant.

The *FB* (or *FB′*) curve is an unstable plasma state, not obtained experimentally. The electrical characteristics of this plasma are essentially the same, with the capacitor formed between the two electrodes. The densities of the charged species are shown in Figs. 3 and 4(b). Notice that although electron densities drop quickly, the ion sheath is still present, and positive-negative ion densities are still of the same order of magnitude. The observed voltage and density behavior, as a function of current density, is very similar to the extinction behavior observed for Ar discharges [19,20].

At point *B* (or *B′* depending on γ), which we denote as the breakdown point, the ion sheath collapses (i.e., becomes greater than half the discharge length), and positive-negative ion densities drop quickly and are of unequal magnitude. The model predicts that *BA* (or *B′A*) is a stable series of states, where a collection of positive and negative ions, and electrons, can exist at small densities; see Figs. 3 and 4(c). After extinction the discharge moves to this stable regime *BA* (*B′A*). Both the Floquet multipliers and time integration show that states from *FB* (*FB′*) collapse onto states on *BA* (*B′A*), but the densities on *BA* (*B′A*) do not become zero with time. This happens only below point *A*. It appears that point *A* is a prebreakdown point, leading not to the formation of a discharge but to a collection of carriers. It is not clear to us whether this behavior is real, an artifact of the boundary conditions [18,20], or an effect of the narrow gap (low *PL* value), which suppresses diffusion controlled breakdown, as discussed in the following paragraph.

Figure 2 shows that breakdown depends on the value of γ (curves *AB* and *AB′*), hinting that breakdown is mobility controlled [30]. This can indeed be verified comparing the reduced field strengths (E/P) predicted from the model, and

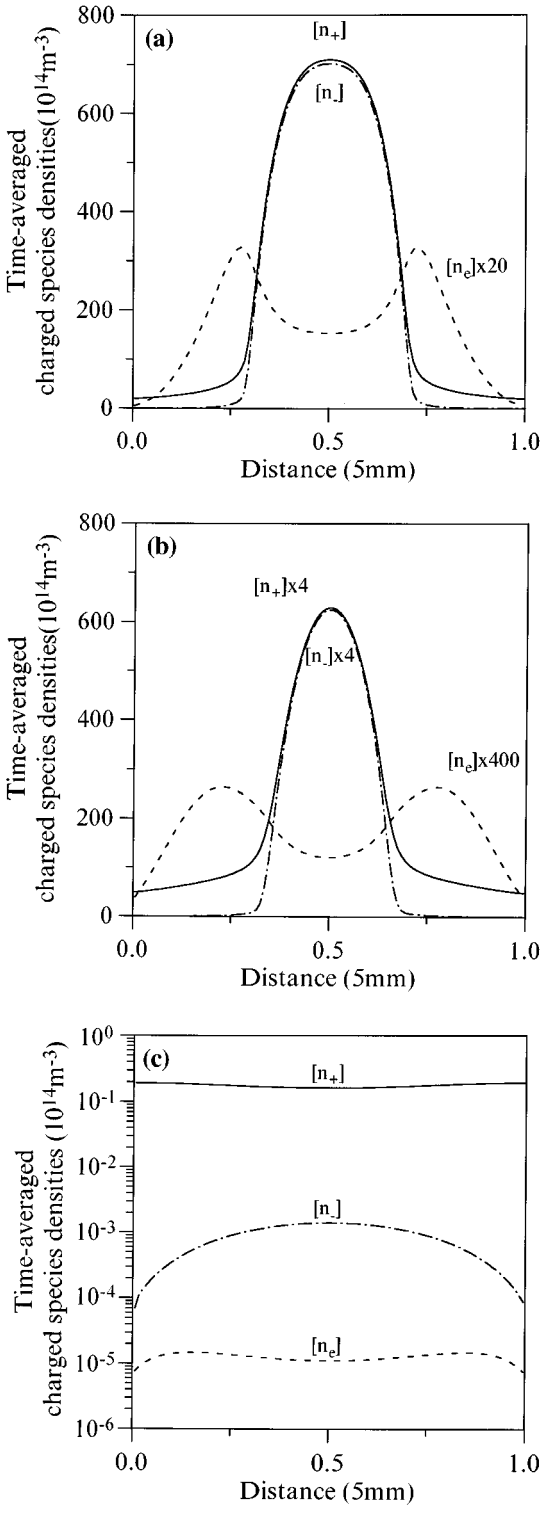

FIG. 4. Electron and ion densities vs the interelectrode position for the three branches, and the same current density ($I=37$ A / m^2): (a) Branch DF stable state, plasma on. (b) Branch FB or FB', unstable state, plasma off. (c) Branch BA or $B'A$, stable state, plasma off.

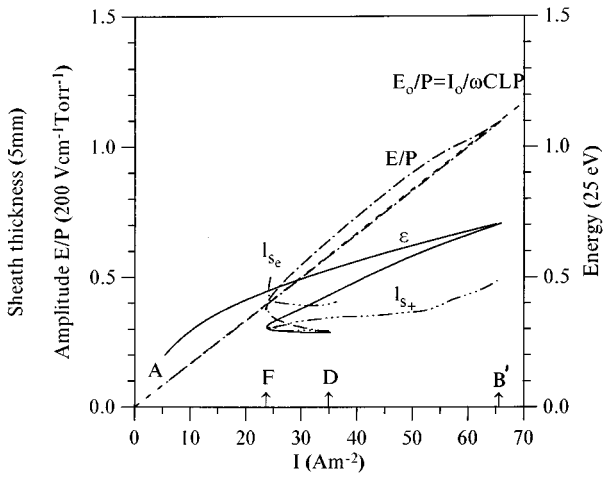

FIG. 5. Electron sheath l_{se} (double-dot—dashed curve), ion sheath l_{s+} (triple-dot–dashed curve), average electron energy in the bulk ε (full curve), E/P ratio in the bulk (dot-dashed curve), and E/P of the capacitor defined by the two electrodes (dashed curve), vs the current density. At the extinction point F, the electron sheath collapses, and at point B' the ion sheath collapses (i.e., they become greater than half the discharge length).

calculated for diffusion- [31] or oscillation-amplitude-controlled [30] breakdown. The model predicts that the E/P amplitude equals 450 V/cm Torr (rms 320) for $\gamma=0.01$, while for $\gamma=0.1$ the E/P is reduced to 250 V/cm Torr (rms 180), for points B' and B, respectively. The E/P in the diffusion-controlled breakdown can be computed [31] balancing electron diffusion plus attachment losses to ionization $[D_e/\Lambda^2=(K_{i(E/P)}-K_{a(E/P)})N]$, while the critical E/P (where the electron oscillation amplitude becomes equal to half the discharge gap L) can also be calculated [30] $[E/P=\pi fL/(2^{0.5}\mu_e P)]$; in the above N denotes the neutral density, K are the ionization and attachment coefficients, D is the diffusivity, L is the discharge gap, $\Lambda=L/\pi$ is the diffusion length, and f is the rf frequency. For $P=2$ Torr, $L=5$ mm, $D_eP=110$ m^2 Torr/s, $\mu_eP=20$ m^2 Torr/V/s, and the ionization/attachment coefficients given by Gogolides, Stathakopoulos, and Boudouvis [17], the calculated rms E/P for a diffusion-controlled breakdown equals 80 V/cm Torr (average electron energy 9.2 eV), while the critical E/P for mobility-controlled breakdown equals 75 V/cm Torr (average electron energy 8.9 eV). Hence the electron oscillation amplitude limit is reached before diffusion breakdown, and the electric field strength required to create the discharge increases sharply, and depends on electrode processes and thus on the value of γ.

To summarize, there exists a hysterisis loop, where the discharge starts at B (B') (breakdown), moves to point E (sustainment or operating point see Fig. 2), and then extinguishes at F. Figure 5 shows the transitions more clearly, as a function of the rf current density amplitude. The maximum electron sheath 1_{se} (i.e., maximum oscillation of the electron front) is plotted, and it is seen to increase quickly at point F, becoming equal to half the interelectrode separation. Conversely, the ion sheath 1_{s+} increases slowly at F, and becomes equal to half the interelectrode separation at B (B'). The time-averaged electron energy ε, and E/P, are also shown, revealing the dramatic increase of both after extinction, since electric fields are not shielded enough after point F, due to the collapse of the electron sheath. On top of the E/P vs I curve of the discharge, the E/P vs I curve of the capacitor defined by the two electrodes ($E/P=I_0/\omega CLP$) is

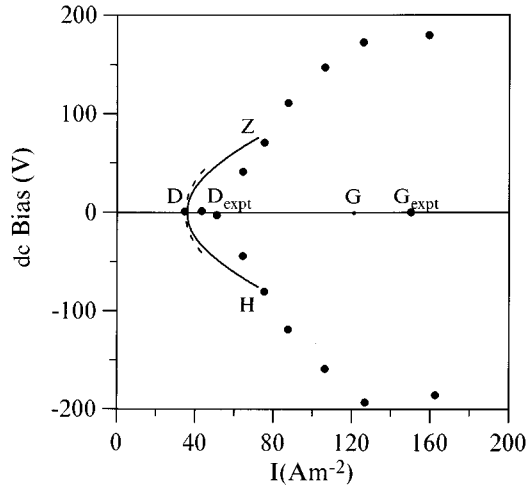

FIG. 6. DC-bias voltage vs current density for $\gamma=0.1$ (full line) and $\gamma=0.01$ (dashed line). Dots are experimental results [1].

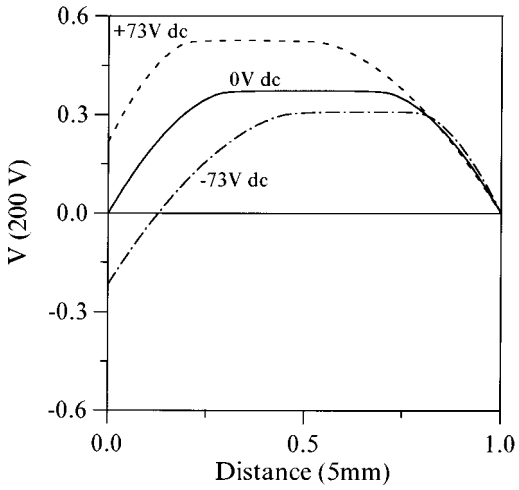

FIG. 7. Potential distribution between the electrodes, for the case of symmetric (0-V dc bias) and asymmetric (+73 and −73-V dc bias) solutions.

plotted, showing its similarity to the plasma characteristics after extinction.

Since we stated that electron oscillation determines the breakdown field in this narrow-gap discharge, it is instructive to calculate the sustainment electric field, by balancing ambipolar diffusion and attachment losses to ionization $[D_a/\Lambda^2=(K_{i(E/P)}\text{-}K_{a(E/P)})N]$. The calculation will permit a comparison of the sustainment E/P predicted by the model, and the one required for a discharge in the diffusion-controlled regime. The value of the ambipolar diffusivity varies depending on the ratio of electron to ion temperature, and the ratio of negative ion to electron densities [31,32]; for the minimum value [attained for very few negative ions, $D_a=D_e/(1+\mu_e/\mu_+)=1/264$] the minimum sustaining electric field is 47 V/cm Torr (average electron energy $\varepsilon=7$ eV). Our model (which includes detachment, and a large number of negative ions) predicts E/P equal to 50 V/cm Torr ($\varepsilon=7.5$ eV) for the center of the plasma (see Fig. 5). The two values are not very different, showing that the discharge can in principle exist with the usual structure of a diffusion-controlled discharge, after its ignition, despite the high E/P required for breakdown.

C. Medium current density region. Development of dc bias in a symmetric discharge

In this section we study the region FDG shown in Fig. 1, in which the dc bias develops. Figure 6 shows the dc self-bias versus the rf current density amplitude. The data from Butterbaugh [1] are also plotted for comparison. Up to point D only one branch of solutions exists with zero dc bias. At higher currents two additional branches develop with a supercritical pitchfork type bifurcation, having positive and negative dc-bias voltages, respectively. The additional branches are stable, while the middle branch becomes unstable. Finally, at even higher currents the branches collapse back into the symmetric solution. Notice from Fig. 2, that the branches with dc bias, for the same current density, show a *higher* rf voltage than the middle symmetric branch. This suggests that the stable discharge state is here the one with *higher impedance*.

Results for two values of γ are plotted in Figs. 1 and 6. Note that the plasma states on the dotted curve ($\gamma=0.01$) remain unstable and asymmetric even for very high values of the current density. However, the states on the full curve ($\gamma=0.1$) become stable after point G, in agreement with the experimental data, which show that at point G_{expt} the two branches with dc bias abruptly disappear, and the discharge becomes symmetric again. The stable states on the curve with $\gamma=0.1$ have now a *lower impedance* compared with those with $\gamma=0.01$.

The agreement with experimental data is satisfactory, given the experimental error and the fact that our values of the dc bias are accurate within 10%. This is so because we are using 100 mesh points and a uniform mesh, when discretizing the differential equations. To reduce the error for the dc bias to below 1%, we needed between 300 and 400 mesh points; however, the computational cost increased prohibitively, and only a few selected points were calculated with higher accuracy. The form of the *V-I* curve did not change as a function of mesh points; however, point D moved to lower values as the mesh points were increased. Our model could not follow the solutions with dc bias above points Z and H (see Fig. 6), due to numerical problems with the time integrator, which could not be circumvented by decreasing its time step.

Having presented the *V-I* characteristics of the branches resulting from the pitchfork bifurcation, we now attempt to explain the discharge structure. Figures 7 and 8 show the time-average potential and electric field distributions for the positive, zero, and negative dc-bias cases respectively. (Electric fields were shifted up and down for the solutions with dc bias to be put in the same plot as the one without dc bias.) The electrode at position $x=1$ (5 mm) is grounded. Note that in comparison with the zero bias case, the thickness of the bulk of the plasma has been reduced, and the sheath adjacent to the more negative electrode became larger; the plasma is now asymmetric. The time-averaged electron densities are shown in Fig. 9, for the three cases of positive, zero, and negative dc bias. Electrons are pushed away from the larger sheath (i.e., the more negative electrode), and toward the

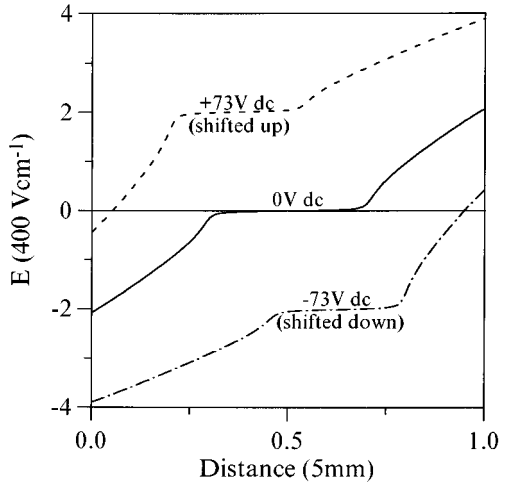

FIG. 8. Electric field vs interelectrode position, for the cases of symmetric (without dc bias) and asymmetric (with dc bias) solutions. The curves with dc bias were shifted up and down from the zero axis in order to be clearly visible; their flat part is at 0 V/cm.

more positive electrode, while the density profiles become asymmetric, resulting in dc-bias formation.

An understanding of the sustainment mechanism of the discharge can be gained from Figs. 10(a)–10(c) and 11(a)–11(c). Figure 10 shows contour lines of the absolute value of the electric field, versus position and rf time (phase) of the applied sinusoidal current density. Note that in addition to the high electric field values on the electrodes, local maxima which correspond to the double layers [22,23,33] are present at the bulk-sheath interface. Double layers are created by the oscillating electrons, as they change the space charge and potential distribution set up by the positive-negative ions, which hardly respond to the field at this frequency. The symmetric plasma has two such double layers [Fig. 11(b)], while in the asymmetric plasmas the double layer close to the more negative electrode disappears [Figs. 10(a) and 10(c)].

In the bulk of the plasma electron energy shows analogous behavior with the absolute electric field, and local maxima in the double layers. Thus the ionization rate constant $K_i(\varepsilon)$, which depends exponentially on energy, will have larger values in the double layers, compared to the bulk. Figure 11 shows as a function of position and time the ionization rate R_i defined as $R_i = K_i(\varepsilon) N n_e$, where N and n_e are the neutral and electron densities, respectively. The first observation is that the ionization peaks coincide with the

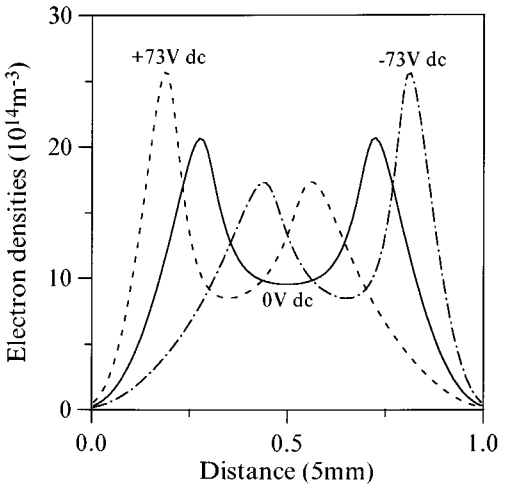

FIG. 9. Electron density time averaged over the rf cycle vs the interelectrode position for the three cases of dc bias.

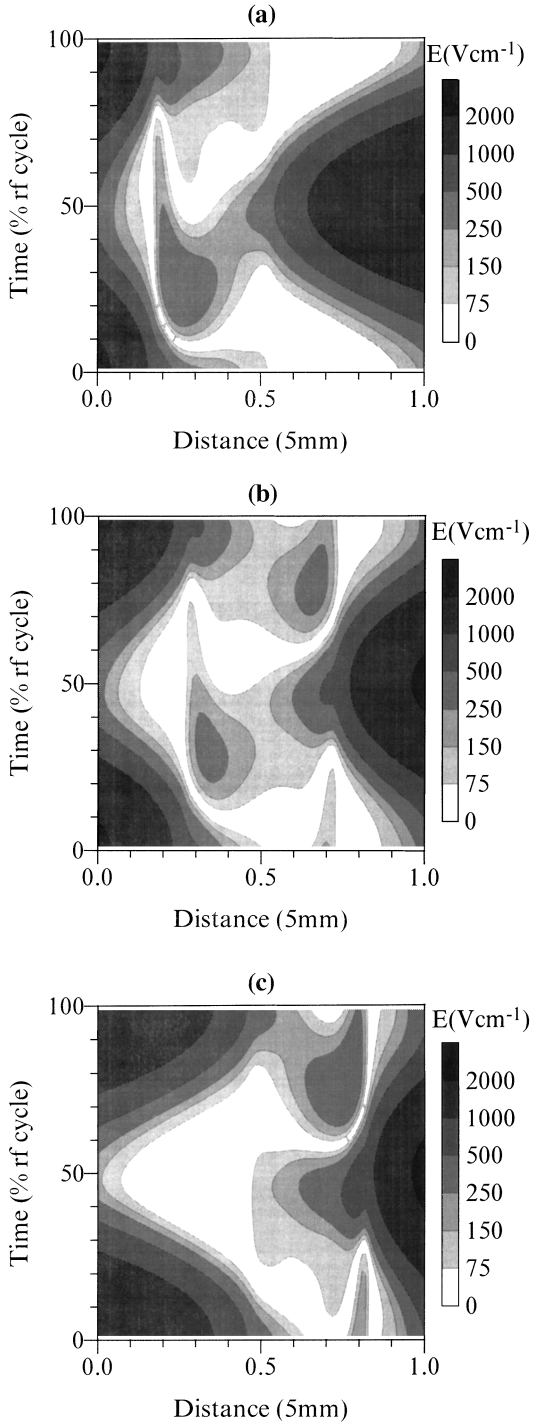

FIG. 10. Contour lines of the absolute value of the electric field vs position and rf time. Darker colors signify higher electric fields. (a) Solution with positive dc bias. (b) Solution with zero bias. (c) Solution with negative dc bias. The darker islands in the plasma bulk ($x = 0.3$–0.4%, $t = 20$–40% and $x = 0.6$–0.7%, $t = 70$–90%) for contour (b) are the double layer regions. Contours (a) and (c) show only one such double layer.

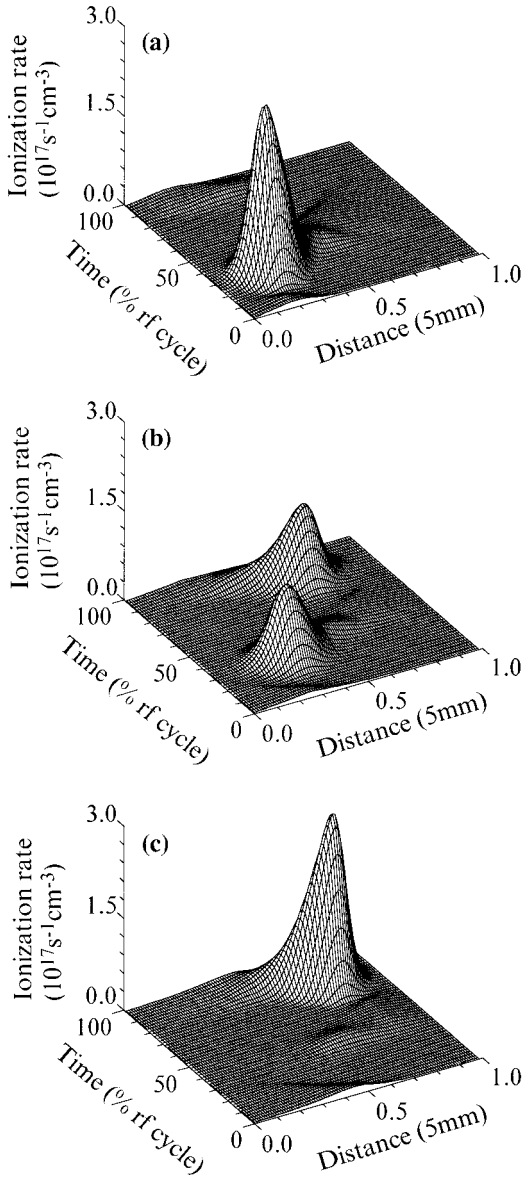

FIG. 11. Three-dimensional view of the ionization rate vs position and rf time. (a) Solution with a positive dc bias. (b) Solution with zero dc bias. (c) Solution with a negative dc bias. The dc bias develops at position 0, while position 1 is grounded. Ionization coincides with the double layers.

position and phase of the local electric field maxima due to the double layers. Hence this narrow-gap (low PL value) electronegative plasma is sustained mostly by double layer ionization: Electrons from the bulk are accelerated toward the sheath and accumulated in the double layer, causing increased local ionization. Conversely, in electropositive discharges, ionization takes place due to electrons, which have diffused in the sheath, and are accelerated back into the bulk of the plasma. Compare Fig. 11(b) with Figs. 6 and 7 from Gogolides and Sawin [18].

The second observation from Figs. 11(a)–11(c) is that the asymmetric plasma with dc bias shows only one ionization peak close to the smallest sheath (i.e., the sheath close to the more positive electrode). The ionization peak close to the more negative electrode has disappeared. Indeed, as the double layer in the sheath close to the more negative electrode disappeared (see Fig. 11), the electric fields, and electron energies became smaller, the ionization rate constant was reduced, and the ionization rate dropped significantly there. Since ionization and light emission are analogous processes, this suggests that emission from one sheath disappears, very much in agreement with the observations of Butterbaugh [1]. Butterbaugh attributed the phenomenon to the disappearance of one sheath, while in reality it is the one double layer which disappears. Finally, notice that, contrary to the usual behavior, where the ionization peak appears close to the electrode with the negative dc bias (e.g., in discharges with unequal size of electrodes), here the ionization peak disappears from the side of the electrode with the negative bias. This is also due to the disappearance of the double layer there.

The asymmetry induced in the discharge from the dc bias inevitably has consequences on the electrical characteristics of the discharge. In symmetric discharges the two equal sheaths oscillate with a phase difference of 180°. As a result, if one applies a sinusoidal voltage (or current), the current waveform (or voltage, respectively) has only odd harmonics. When this symmetry was broken, the waveform contained even harmonics as well [1]. In the model a current was forced in the discharge, and the voltage waveform was found to contain all harmonics, the second harmonic being twice as large as the third one, and about 3% of the first harmonic.

In an effort to explain the observed phenomena we varied the electrode spacing, the pressure, and the electron mobility. We observed that the dc bias drops with increasing pressure or increasing space (i.e., increasing PL) in agreement with experiments [1], and for the spacing of 5 mm, it *disappears*, when a constant instead of a variable electron mobility is used (see Sec. II). We changed the electron mobility function to a constant, with values ranging from $\mu P = 20$ to 100 m^2 Torr/V/s. Starting from any asymmetric solution, obtained with the variable mobility function, changing to a constant mobility and integrating in time resulted in a symmetric solution for $\mu P < 60$ m^2 Torr/V/s, or to discharge extinction for higher mobility values. We thus concluded that it is the functionality of μP with electron energy ε, which is probably responsible for the observed phenomena. This functionality yields high mobilities at low ε (or E/P), and traces back to the momentum transfer cross section dependence with ε, which for CF_4 shows a minimum. Close to the electrodes we observed very low electron energies during parts of the rf cycle, when electrons diffused in the sheath (2.5–3.5 eV); the resulting mobilities were as high as 140 m^2 Torr/V/s, resulting in high diffusivities, and hence increased diffusion fluxes and enhanced losses of electrons on the electrodes (see Sec. II). Consequently electrons could be randomly lost on the powered or grounded electrode, depending on the phase of the cycle. If electrons were to be randomly lost on the powered electrode, they would cause the appearance of a negative dc bias, the increase of the powered sheath, the shrinking of the bulk region, and the accumulation of the electrons in the double layer adjacent to the grounded electrode. Should our hypothesis be true that the observed phenomena are due to the minimum in the momentum transfer cross section in combination with the electronegativity of the plasma, other gases or gas mixtures with

similar mobility functions and electronegativity should show analogous behavior. The electronegativity is thought to be important for the results discussed in this work, since the formation of double layers and relevant phenomena are a characteristic of electronegative plasmas.

D. High current density region

As discussed previously, the high current density region depends on the value of the secondary emission coefficient. If the secondary emission is not enough to balance the loss of electrons on the electrodes due to their oscillation, then the discharge is unstable. If there are enough electrons, then the symmetric discharge becomes stable, and the plasma bulk can expand again. For the case of high γ we observed increased ionization in the sheaths and in the bulk. Although our model can handle the α to γ transition, its accuracy must be checked since we are using one energy to characterize all electrons, and underestimate the highly energetic beam electrons which cause the transition.

IV. CONCLUSIONS

Using a fluid model, the behavior of the CF_4 discharge in a narrow-gap (low PL value equal to 1) reactor of 5 mm was investigated as a function of applied rf current density at 2 Torr. For low current densities two turning points exist in the V-I curve, one corresponding to the extinction of the plasma and the expansion of the electron sheath to the whole discharge region, and the other corresponding to breakdown. These two points define a hysterisis loop. Breakdown at such low PL values is mobility controlled, and depends on the value of the secondary emission coefficient γ.

For medium currents the V-I characteristic exhibited a pitchfork bifurcation leading to the appearance of two stable asymmetric branches with dc bias, under symmetric reactor configuration. The asymmetry was also shown by asymmetric ionization and emission profiles, and by the disappearance of one of the two double layers. These results are in agreement with experimental data [1]. The value of the dc bias depended on γ, electrode spacing, pressure, the formation of double layers (i.e., electronegativity), and the functionality of the electron mobility with electron energy resulting from the dependence of the momentum transfer cross section with energy.

Finally, at high currents secondary electron emission becomes again important, and for $\gamma=0.1$ the asymmetric branches collapses again on a symmetric solution. It is indeed important to note that a one-dimensional fluid model can capture discharge nonlinearities, and phenomena which one would intuitively tend to consider as two dimensional, such as the appearance of solutions with dc bias in symmetric systems.

ACKNOWLEDGMENTS

We thank Professor H. H. Sawin and J. Butterbaugh for providing a copy of Dr. Butterbaugh's thesis, and the Supercomputing Centers of NCSR Demokritos and of the National Technical University.

[1] J. Butterbaugh, Ph.D. dissertation, Massachusetts Institute of Technology, 1990.
[2] V. I. Kolobov and A. Fiala, Phys. Rev. E **50**, 3018 (1994).
[3] K. G. Muller, Phys. Rev. A **37**, 4836 (1988).
[4] Z. Lj. Petrovic and A. V. Phelps, Phys. Rev. E **47**, 2806 (1993).
[5] B. M. Jelenkovic, K. Rozsa, and A. V. Phelps, Phys. Rev. E **47**, 2816 (1993).
[6] A. V. Phelps, Z. Lj. Petrovic, and B. M. Jelenkovic, Phys. Rev. E. **47**, 2855 (1993).
[7] P. G. Daniels, R. N. Franklin, and J. Snell, J. Phys. D **23**, 823 (1990).
[8] R. N. Franklin, P. G. Daniels, and J. Snell, J. Phys. D **26**, 1638 (1993).
[9] J. R. M. Coulter and K. G. Emeleus, Int. J. Electron. **64**, 961 (1988).
[10] D. B. Ogle and G. A. Woolsey, J. Phys. D **20**, 453 (1987).
[11] G. A. Woolsey, K. G. Emeleus, J. M. Brown, J. J. G. McCloskey, and J. R. M. Coulter, Int. J. Electron. **19**, 485 (1967).
[12] W. L. Nighan and W. J. Wiegand, Phys. Rev. A **10**, 922 (1974).
[13] Yu P. Raizer and M. N. Shneider, J. Phys. D **27**, 1457 (1994).
[14] I. D. Kaganovich, Plasma Phys. Rep. **21**, 434 (1995).
[15] E. S. Aydil and D. Economou, J. Appl. Phys. **69**, 109 (1991).
[16] P. A. Miller and K. E. Greenberg, Appl. Phys. Lett. **60**, 2859 (1992).
[17] E. Gogolides, M. Stathakopoulos, and A. Boudouvis, J. Phys. D **27**, 1878 (1994).
[18] E. Gogolides and H. H. Sawin, J. Appl. Phys. **72**, 3971 (1992).
[19] E. Gogolides and H. H. Sawin, J. Appl. Phys. **72**, 3988 (1992).
[20] E. Gogolides, H. H. Sawin, and R. A. Brown, Chem. Eng. Sci. **47**, 3839 (1992).
[21] B. Chapman, *Glow Discharge Processes* (Wiley, New York, 1980).
[22] S. Kakuta, Z. Lj. Petrovic, F. Tochikube, and T. Makabe, J. Appl. Phys. **74**, 4923 (1993).
[23] Z. Lj. Petrovic, F. Tochikubo, S. Kakuta, and T. Makabe, J. Appl. Phys. **73**, 2163 (1993).
[24] N. V. Mantzaris, A. Boudouvis, and E. Gogolides, J. Appl. Phys. **77**, 6169 (1995).
[25] J. H. Bolstad and H. B. Keller, Siam J. Sci. Stat. Comput. **7**, 1081 (1986).
[26] H. B. Keller, in *Applications of Bifurcation Theory*, edited by P. Rabinowitz (Academic, New York, 1977), pp. 359–384.
[27] A. G. Boudouvis, Ph.D. dissertation, University of Minnesota, 1987.
[28] R. Seydel, *From Equilibrium to Chaos, Practical Bifurcation and Stability Analysis* (Elsevier, New York, 1988).
[29] I. G. Kevrekidis, L. D. Schmidt, and R. Aris, Chem. Eng. Sci. **41**, 1263 (1986).
[30] S. C. Brown, *Introduction to Electrical Discharges in Gases* (Wiley, New York, 1965).
[31] A. T. Bell, in *Techniques and Applications of Plasma Chemistry*, edited by J. R. Hollahan and A. T. Bell (Wiley, New York, 1974), pp. 1–56.

[32] A. G. Lichtenberg, V. Vahedi, and M. A. Lieberman, J. Appl. Phys. **75**, 2339 (1994).
[33] J. P. Boeuf and Ph. Belenguer, in *Non-Equilibrium Processes in Partially Ionized Gases*, Vol. 220b *NATO Advanced Study Institute Series*, edited by M. Capitelli and J. M. Bari (Plenum, New York, 1990), p. 155.